



Effects of the configuration of a baffle–avalanche wall system on rock avalanches in Tibet Zhangmu: discrete element analysis

YuZhang Bi¹ · SiMing He^{2,3,4} · YanJun Du¹ · XinPo Sun⁵ · XinPo Li^{2,4}

Received: 20 September 2017 / Accepted: 4 April 2018 / Published online: 10 May 2018
© Springer-Verlag GmbH Germany, part of Springer Nature 2018

Abstract

Rock avalanches with a high mobility and kinetic energy pose a potential geological risk to surrounding buildings. Baffles and avalanche walls are effective ways to protect these buildings. However, the primary focus of previous studies has been on baffles or avalanche walls alone, and there have been very few studies investigating the effectiveness of a combination of baffles and avalanche walls as a countermeasure against rock avalanches. In addition, previous studies on lab-scale tests and numerical analyses often did not take the actual topography effects into consideration. In this study we adopted a numerical simulation approach based on an actual project in the town of Zhangmu, Tibet, with the aim to investigate the effect of different configurations of a combined baffle–avalanche wall system on impeding the kinetic energy of rock avalanches. A series of numerical analyses with discrete element methods (DEM) were conducted. First, the effect of three different pile groups on the reduction of the effect of the rock avalanche was studied using the numerical modeling study. Secondly, the influence of the size of the retaining wall on the maximum impact force of the rock avalanche was studied. Finally, a DEM modeling study on the energy dissipation capacity of the baffle–avalanche wall system was conducted. The results demonstrate that an arrangement of different baffle–avalanche wall systems will produce different results in terms of dissipating the energy of rock avalanches: when the wall is long enough to block all rock masses, enhancing baffle density will decrease the maximum impact force exerted on the avalanche wall; however, if the wall is just long enough to protect the target region, reducing baffle density will decrease the maximum impact force exerted on the avalanche wall. The results of this study are significant in terms of providing guidelines for the design of baffle–avalanche wall systems for protection against rock avalanches.

Keywords Rock avalanches · Baffles · Interaction mechanisms · Zhangmu · Energy dissipation

Introduction

A rock avalanche is defined an extremely rapid, massive, flow-like motion of fragmented rock from a large rock slide

or rock fall (Hungre et al. 2014). The most common causes (triggers) of rock avalanches are earthquakes, rainfall, freeze–thaw, weathering, as well as other environmental and man-made factors, and they are usually accompanied by gravity or other external forces generated by rock joints (Hungre and Evans 2004; Strom 2004; Cox and Allen 2009; Grämiger et al. 2016). Rock avalanches are common geological hazards in the southwest mountainous area of China, where they are characterized by their high kinetic energy and potential for inflicting destruction (Qi et al. 2011; Bi et al. 2016b). Much research has been carried out on the dynamic mechanisms of the space and time of the rock avalanches, including in situ tests (Azzoni and De Freitas 1995), model experiments (Davies and McSaveney 1999), theoretical solutions (Denlinger and Iverson 2004), and simulations (Davies and McSaveney 2002). In situ tests and model experiments are the two most direct methods commonly used, but they are limited due to their high cost and the weakness of the test results in terms of representation and promotion. Many factors

✉ YuZhang Bi
biyuzhang@seu.edu.cn

¹ Institute of Geotechnical Engineering, School of Transportation, Southeast University, #.2, Sipalou Road, Nanjing 210096, China
² Key laboratory of Mountain Hazards and Earth Surface Process, Chinese Academy of Science, Chengdu 610041, Sichuan, China
³ Center for Excellence in Tibetan Plateau Earth Sciences, Chinese Academy of Sciences, Beijing 100101, China
⁴ Institute of Mountain Hazards and Environment (IMHE), Chinese Academy of Sciences, Chengdu 610041, Sichuan, China
⁵ School of Civil Engineering and Architecture, Southwest University of Science and Technology, Mianyang 621000, Sichuan, China

influence the trajectory characteristics of a complex slope and rockfall, and the form of motion is very complicated. It is difficult to solve the path equation and its parameters accurately by the theoretical analysis method. The numerical method has been applied in recent years because of its low cost, convenient application, and ability to simulate complex problems (Mollon et al. 2015; Xing et al. 2017; Li et al. 2017).

Engineers have proposed various structures to reduce the damage to infrastructure caused by a rock collapse and to protect residential areas and the traffic routes downstream of the disaster, such as shed galleries (Bi et al. 2016b), baffles (Ng et al. 2015), and avalanche (retaining) walls (Li et al. 2010); all such structures have been widely applied. The shed gallery is considered to be a form of protective structure that is often used as protection against rock disasters. However, it is mainly suitable for the protection of traffic routes and has not seen overall implementation. The retaining wall has a very good effect on the energy consumption of a rock avalanche and is a suitable structure for the protection of residential areas, but its cost is too high for wide applicability, and the strength of the concrete is an important influencing factor. Compared with other disaster prevention structures, the baffle has become the more acceptable disaster prevention structure due to its low cost and high adaptability, especially in steep mountainous areas (Bi et al. 2018). This structure has a number of advantages, and many researchers have launched a series of studies on arrays of baffles as a means for protection against rock avalanches. Cosenza et al. (2006) installed baffles in a basin to mitigate debris flow and proved that the slippage of the debris flow was well reduced by the system of baffles. Ng et al. (2014) conducted a series of laboratory experiments to study the interaction between debris flow and baffles and found that there was a need to pay attention to the height of the baffles during the design of the system as height was essential for controlling the slippage of debris flow. Choi et al. (2014) also conducted a series of numerical simulations to study the relationship between baffle configuration and impedance of channelized debris flow. However, the scale of the experiment was too small for the results to be meaningful to a real situation.

Many of the studies conducted to date on the interaction between baffles and rock avalanches, including experiments and simulations, have been at small scales and, therefore, the results do not reflect the effects of the actual terrain. Also, when an actual project is being considered, it is not sufficient to use only a baffle group approach; diversified protective measures need to be considered to protect against a disaster.

In the study reported here, we used the actual conditions and the actual terrain as the research background and apply discrete element modeling (DEM) as the main method to achieve the aim of the experiment. Using the actual working conditions of the Zhangmu disaster in Tibet, we study the

influence of the arrangement of “a baffles–wall hybrid protective structure” on disaster mitigation and provide technical guidance for disaster prevention and mitigation of the effects of a rock disaster.

In this paper, we first provide a brief introduction on the terrain features and geological conditions. Secondly, we report on our study of the effect of baffle structure on reducing the effects of the rock disaster, based on three different conditions of actual working conditions. Thirdly, the numerical analysis is used to study the law of impact force that rock avalanches exerted on retaining walls as influenced by different wall size. Finally, the structure of the avalanche (retaining) wall is added to the model to optimize the baffle design. A series of studies are carried out with the “pile-wall” hybrid system combined with actual engineering activities.

Background

The potential for catastrophic landslides around the town of Zhangmu, Tibet, is very high and is dependent on the trigger conditions, such as earthquake, rainfall, among others. Hence, it is necessary to add protective structures in these regions to protect the target regions, such as residential areas, against the destructive impact of this geo-hazard.

Engineering generalization

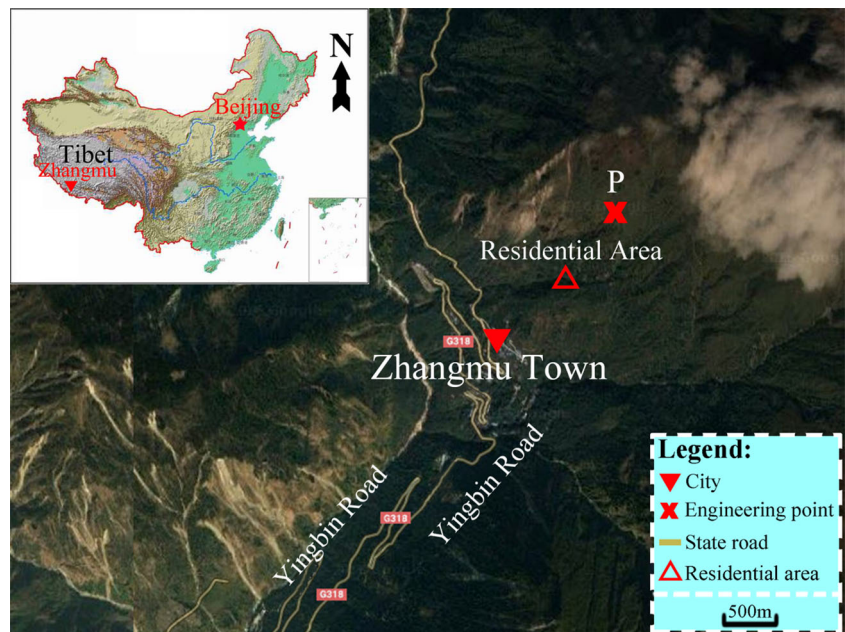
Topographic and geomorphologic conditions

The town of Zhangmu is located on the southern slope of the left bank of the Qubo River, in the southwest area of the Tibet Autonomous Region; specifically, on the southernmost part of the Qinghai–Tibet Plateau, located on the southern slope of the Himalayas. The main morphostructure was formed from intense lifting of the mountains and a deeply incising effect of streams, resulting in the creation of many cliffs in this region. As shown in Fig. 1, the engineering site (P on Fig. 1) is located to the northeast of the town of Zhangmu and is characterized by steep terrain and an unstable rock distribution. The residential area is located downstream of potential avalanches. It is the main protection target of the engineering project; the Yingbin road, which is across from the town of Zhangmu, is the secondary protection target. The residential area is located between camphor and the engineering points, downstream of the potential debris flow. The horizontal and vertical distances from the target source area to the residential area are 70 and 120 m, respectively.

Slope structure

The project is located in the northeast of China’s Tibet Zhangmu town (85°58′59″ E, 27°59′14″ N). The

Fig. 1 Topography of the area around the town of Zhangmu and identification of the main protection targets. *P* location of the study site



geological structure of the source area is mainly granite. As shown in the cross-sectional view (Fig. 2), the maximum elevation of the source area is 2710 m a.s.l., and the elevation of the residential area and the slope foot are 2592 and 2520 m a.s.l., respectively. Figure 2 also shows the upper terrain is very steep (45–60°) and that the lower terrain is relatively gentle (5–10°). The field measurement reveals that there is a potentially dangerous rock area of about $0.3 \times 10^5 \text{ m}^3$ and that the elevation of the dangerous rock area is between 2685 and 2740 m a.s.l.

Geological condition

The distribution of the source region is similar to a triangular shape, and the source area to the northwest is higher than that to the southeast. The morphostructure of the potentially detached rock is very steep, and this rock is located at a much higher elevation than the town of Zhangmu, thus leading to a condition of high potential energy. According to the stability analysis, hazard level, and fragmental degree, the source area can be divided into two sections, namely, an instability section and an under-stable section (Fig. 3). The distribution of the unstable region is close to the quadrilateral. The elevation distribution in this section is between 2710 and 2740 m a.s.l. The size of the maximal rock in the area is $7.5 \times 5 \times 2.5 \text{ m}$. The under-stable region is distributed in the shape of a subtriangle. The elevation of the region ranges from 2685 m to 2710 m a.s.l. Depositions from ancient landslides are distributed around this region such that there is an amount of rock mass embedded in the surface of the slope that has low stability. However, a slide is not likely

to be triggered until external conditions are exerted, such as earthquake and rainfall.

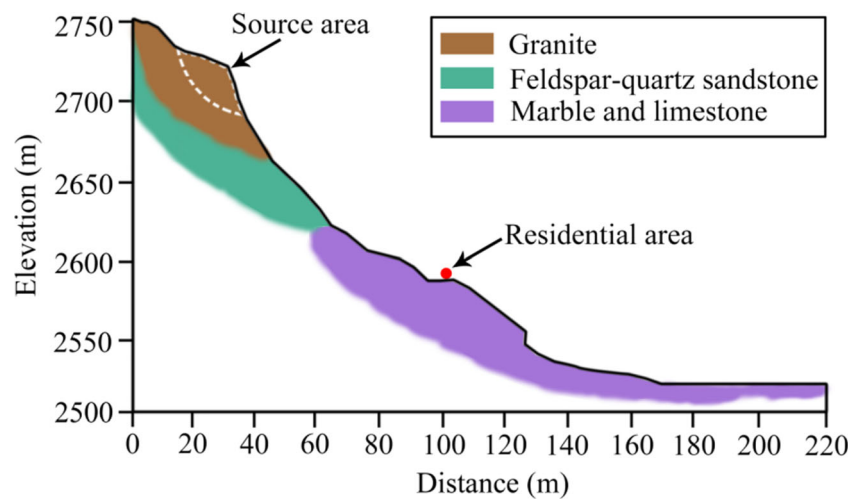
Baffles–wall mixed system

The potential avalanche hazard is an enormous threat to the residential area downstream; therefore, it is necessary to set up a baffles–wall mixed system in this area. A baffles–wall mixed system not only includes such baffles as the traditional baffle protection countermeasure, but also includes an avalanche (retaining) wall that provides a wide range of protection. Figure 4 provides a view of the general set-up of a protection system of baffles and a retaining wall when this system is used in practical engineering. Baffles–wall mixed systems as a countermeasure to rock avalanches effectively integrates the two separate countermeasures (the array of baffles and the retaining wall): the array of baffles effectively consumes the kinetic energy of the avalanche, and the retaining wall protects the target structures. Consequently, the final impact force of the rock avalanche exerted on the retaining wall will be reduced by its passage through the array of baffles. It should be noted that materials of lower strength can then be used to build the retaining wall, thus reducing the cost of the wall.

Numerical model set-up and parameter identification

For the investigation of rock avalanches flowing down a practical slope impinging on defending structures (baffles, avalanche walls) with the DEM modeling, the parameters in the

Fig. 2 Longitudinal cross-section of point P in Fig. 1



DEM models need to be first identified by comparing the numerical results with the results from some benchmark experiments.

Contact law applied to the numerical model

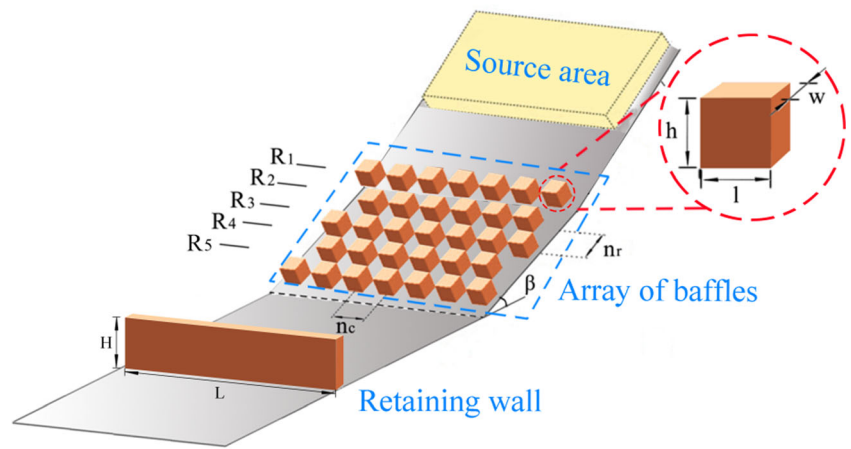
The numerical calculations were performed using the commercial software package Particle Flow Code in three dimensions (PFC3D; Itasca Consulting Group, Inc., Minneapolis, MN, USA), a simulation tool based on the DEM for modeling the dynamic motion and interaction of assemblies of arbitrarily sized spherical particles. The discrete elements, so-called balls, interact with each other by the force-displacement law and Newton's second law of motion (Cundall and Strack 1979).

In this study, a linear rolling resistance model was applied to model the contact behavior of solid particles. This model is based on the linear model, with the addition of a rolling resistance mechanism. It can be installed at both ball-ball and ball-facet contacts. The effect of rolling resistance at contacts between particles, and associated energy dissipation, may be of major importance to many granular applications in both dense, quasistatic, and dynamic regimes. In real granular systems, these mechanisms may have different micro-mechanical origins, such as adhesion of the contact area or the steric effect due to surface roughness or non-sphericity about the contact point. The rolling resistance contact model provided in PFC3D is a simple model that is based on the linear model and it incorporates a torque acting on the contacting pieces to counteract

Fig. 3 Distribution of source area and residential area. *A* Instability section, *B* under-stable section



Fig. 4 Illustration of the “avalanches-baffles-wall” model



rolling motion. It is based on the review paper by Ai et al. (2011) and on the work presented in Wensrich et al. (2012).

The force-displacement law for the rolling resistance linear model updates the contact force and moment as follows (Itasca 2016):

$$F_c = F^l + F^d, \quad M_c = M^T$$

where F^l is the linear force, F^d is the dashpot force, and M^T is the rolling resistance moment.

The rolling resistance linear model provides two additional energy partitions: (1) rolling strain energy, E_{kr} , stored in the linear spring; and (2) rolling slip energy, E_{μ_r} , defined as the total energy dissipated by rolling slip. The whole energy partitions in the rolling resistance linear model are summarized in Table 1.

Numerical modeling

In order to increase the certitude in this study, the numerical model is completely identical to the practical engineering parameters. Three important issues needed to be resolved in the numerical modeling: the topography, the rock avalanches, and the defending structures.

- The topography: The surface of slope is created by the wall-element in PFC3D; in addition, the topography

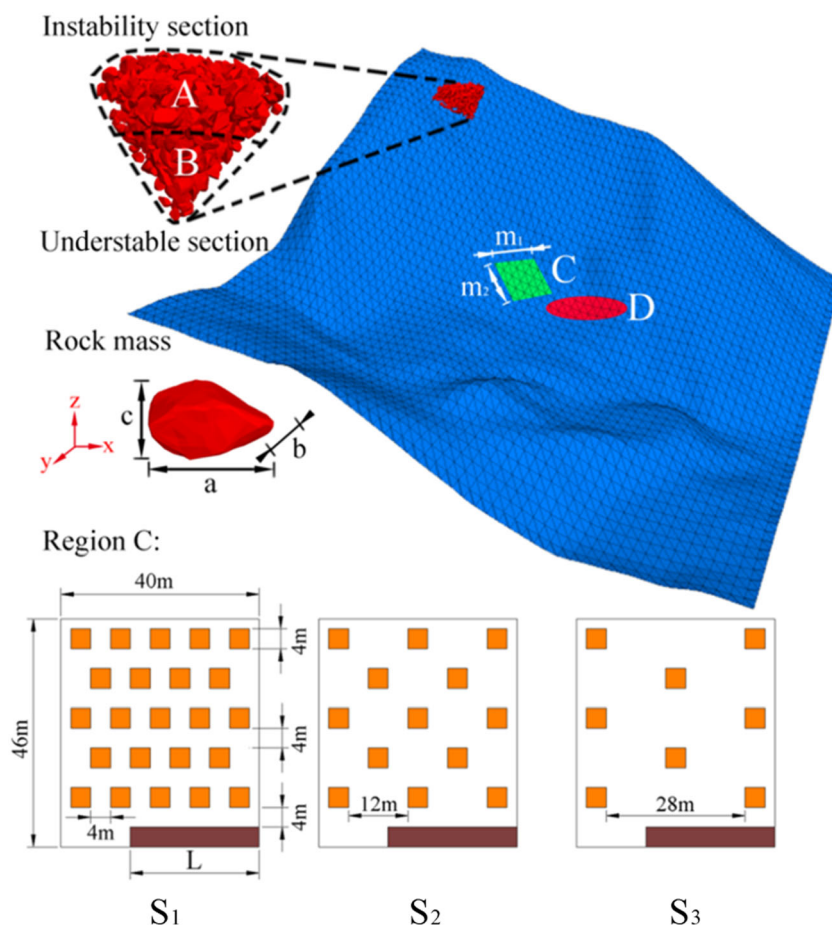
created in numerical modeling is in complete accordance to the situation of the actual topography.

- The rock avalanches: That the mechanisms of flowing mobility for the granular flow of uniform grains are quite different from those of particles of different sizes has been proven by many scholars. It is also known that the shapes of the grains can greatly affect the mechanisms of an avalanche’s kinematics. Hence, the actual shape according to real rock mass has been considered in this study. Figure 5 shows that the length, width, and height of the rock mass are $a = 2.8$ m, $b = 1.6$ m, $c = 0.8$ m, respectively (Fig. 5).
- The defending structures: The region where the defending structures are installed is just along the avalanche’s direction, between the source area and residential area. The defending structures consist of two parts: the array of baffles and the avalanche (retaining) wall. The structures installed in region C and their arrangements are shown in Fig. 5. Three kinds of formats with respect to baffle arrangement are considered, with the avalanche wall added to the protection system in an additional study. Two modifications of the avalanche wall are considered in this study: (1) one long enough to block all of the rock mass that passes thorough the array of baffles to protect the residential area; (2) one just long enough to block part of rock mass but including the residential area in its protection area.

Table 1 Rolling resistance linear model energy partitions

Model group	Description	Symbol
Linear group	Total energy dissipated by slip	E_{μ}
	Strain energy	E_k
Dashpot group	Total energy dissipated by dashpots	E_{β}
Rolling resistance group	Total energy dissipated by rolling slip	E_{μ_r}
	Rolling strain energy	E_{kr}

Fig. 5 Geometry of the actual slope, configurations of baffles (S_1 , S_2 , S_3) and rock avalanches in Particle Flow Code in three dimensions (PFC3D) software



The height of structures is also a key factor that can affect the simulation results. Ng et al. (2015) have proven that the flow velocity decreases with increasing baffle height. Choi et al. (2014) have also reported a series of results showing that tall baffles can more effectively suppress downstream discharge and reduce overflow than shorter ones. For these reasons, we chose sufficiently high baffles and walls (height 10 m) for the numerical models.

Parameter identification

Micro- and macro-parameters are key elements in numerical simulations and will greatly affect the final outcomes in simulation tests. Thus, it is necessary to confirm the proper values of the parameters before the numerical experiments are conducted. In previous studies, some researchers selected parameters based on their own practical engineering experiences (He et al. 2015; Liu and He 2018), while others were inclined to follow the results of predecessors (Bi et al. 2016b). The most commonly used method to acquire parameters is back-analysis (Ulusay et al. 2007; Tokashiki and Aydan 2011; Aydan 2016). However, the back-analysis parameters acquired through continuous

mechanics do not apply to those in DEM simulations (Cundall and Strack 1979). Thus, many researchers often conduct a parameter study with a DEM simulator before starting the follow-up case studies (Li et al. 2010; Bi et al. 2016a). One standard method used to identify the parameters is to adapt to some extent the numerical outcomes with laboratory results, such as angle of repose in sand-piles experiments. In addition, the calibration procedure has been simplified and improved by some scholars.

Rock parameters

Many researchers have conducted studies on rock parameters, with some studies proving that the macroscopic behavior corresponded very well between DEM simulations and real rocks. We performed a series of biaxial numerical tests on granular samples to derive the rock mechanical macro-properties of the granular mixture. Because no one theory can reliably predict macroscopic behavior from microscopic properties and geometry, a trial-and-error process was involved in the numerical tests (Fig. 6). The material constants adopted for the DEM simulations are summarized in Table 2. In particular, the values of the inter-particle friction angle used

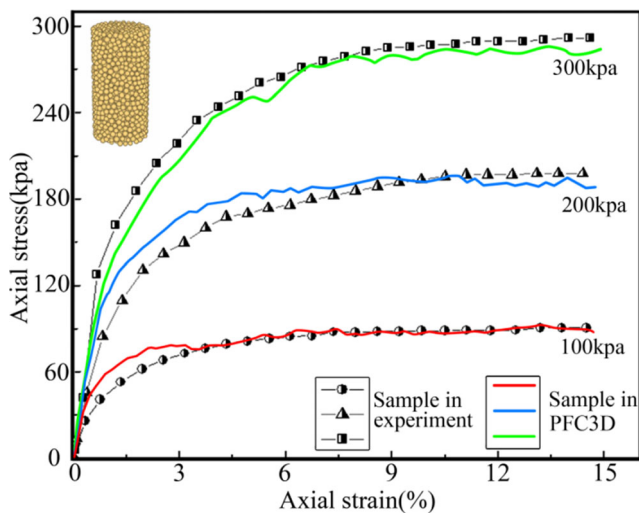


Fig. 6 Comparison between laboratory experiment and the discrete element modeling (DEM) simulation with compressive strength tests

by Salciarini et al. (2009), calibrated using the linear correlation between φ_{μ} and the macroscopic friction angle φ as proposed by Li et al. (2010), were adopted in this study.

Slope friction coefficient

The vegetation in this area is mainly *Kobresia humilis*, commonly found in alpine meadows, and is widely distributed on the slope. The alpine shrub *Entilla fruticosa* is also distributed throughout this area, but as the main vegetation type is alpine meadow, this latter alpine shrub will not be considered in the numerical studies, which will simplify the engineering problems and ensure that our study focuses the discussions on the efficiency of the defending structures. In addition, by the ignoring the shrub factor, the outcomes will be more conservative (the impact force is larger, the structural strength is bigger), which benefits engineering safety.

The numerical results in the smooth slope are much different from those in the slope with full vegetation coverage. Under this consideration, it is necessary to ensure a reasonable slope friction coefficient in the PFC3D. Bi et al. (2016b) conducted a series of comparison studies between laboratory and

Table 2 Parameters of rock, as suggested by the results of a series of biaxial tests

Parameter	Magnitude
Ball stiffness K_N, K_T (N/m)	4×10^7
Wall stiffness K_N, K_T (N/m)	4×10^7
Number of discs	5606
Particle density (kg/m^3)	2700
Contact friction angle φ	38°
Local damping α	0.1
Viscous damping β_m	0.3

numerical experiments to determine the proper parameter values of the slope friction coefficient. However, the outcome of the slope friction coefficient derived from numerical experiments conducted in PFC2D by Bi et al. (2016b) is not suitable for use in the present study. In order to obtain accurate parameters, numerical experiments need to be conducted in PFC3D and matched with the laboratory results. As shown in Fig. 7, the vegetation-covered slope model had a height of 1.8 m and a length of 1.9 m. The rockfall model, whose shape is close to sphere, had a radius of 0.02 m and a weight of 98 g. Furthermore, the same model of slope and rockfall was set up in PFC3D to ensure the accuracy of the numerical outcome. Taking into account the comparison between rockfall trajectories in the laboratory and numerical experiments, the final change rule is shown in Fig. 8. A series of comparisons of the rockfall trajectory on the slope's surface between the experiment and PFC3D is also shown in Fig. 8, and these comparisons confirm that the rockfall trajectory in PFC3D corresponds with the trajectory in the experiment and that the slope friction coefficient is 1.5.

Particle friction coefficient

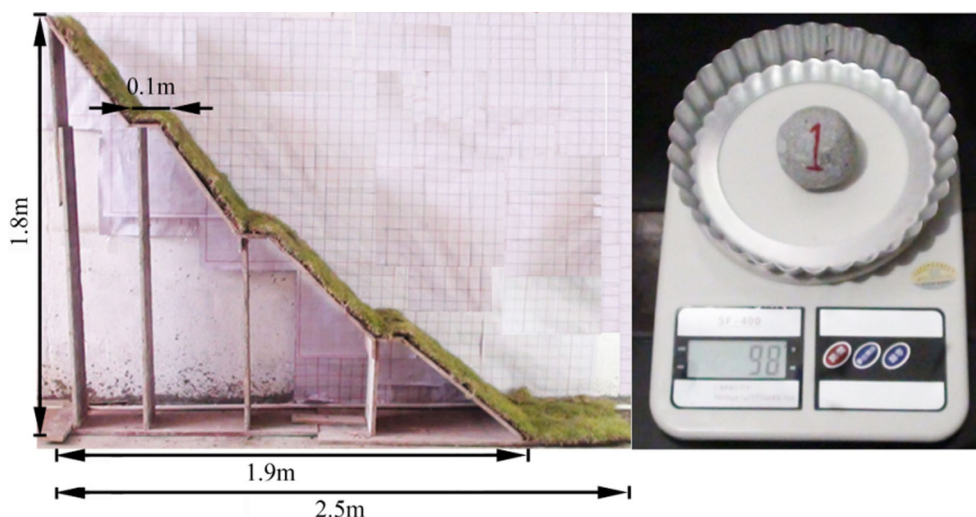
There are two kinds of particle friction coefficients in the rolling resistance linear model: the friction coefficient in linear group μ , and the rolling friction coefficient μ_r in rolling resistance group (see Table 1). To determine these two parameters, we conducted a series of experimental studies on the collapse of granular columns. Figure 9 shows the experimental device used, which consists of a 0.08-m-high cylinder of inner radius R_1 resting on a horizontal polyvinyl chloride plane. The tube is filled with a volume V_0 of granular material. The experimental procedure simply consists of quickly removing the tube by means of a lifting system made of rope and pulleys. After it is released, the granular column spreads on the horizontal plane until it comes to rest and forms a deposit. The type of granular material is granitic particle because the situ rock is granite. The mean grain size is 3.0 mm.

Figure 10 shows that the final deposition of granitic particles in the laboratory experiment of granular columns collapses. The repose angle is 18° . Figure 11 shows the variation in the repose angle with changes in the value of rolling friction coefficient μ_r under conditions of two kinds of friction coefficient μ . It can be seen from this figure that the repose angles are determined by these two factors. The corresponding particle friction coefficient of repose angle 18° are $\mu = 0.25$, $\mu_r = 0.5$ at the same time.

Results and discussion

In the framework of practical engineering, first consideration needs to be given to three key factors in a baffle–wall mixed

Fig. 7 Experimental installation. Left: Slope model, right: rockfall model (Bi et al. 2016b)



configuration. First, the baffles–wall configuration is a defense system; consequently, one of the foremost considerations must be given to its ability to dissipate energy. Second, consideration must be given to the affected area when avalanches pass through the different baffle configurations. Last, but not least, the effect of baffle configuration and its damage resistance is also crucial, especially from the point of view of the engineering budget. However, it is still open to debate whether an optimal scheme can be determined by only taking into account these three elements. Some researchers (e.g., Jóhannesson et al. 2009) also point out that the height of the obstacle is an essential element to prevent supercritical overflow. However, in this study, obstacle height is assumed to be sufficiently high in order to simplify the research questions.

To obtain a suitable design scheme to prevent potential hazards, we studied baffle configuration, wall configuration, and baffles–wall mixed configuration.

We considered the baffle configuration problem to be the most important challenge and analyzed this problem in three

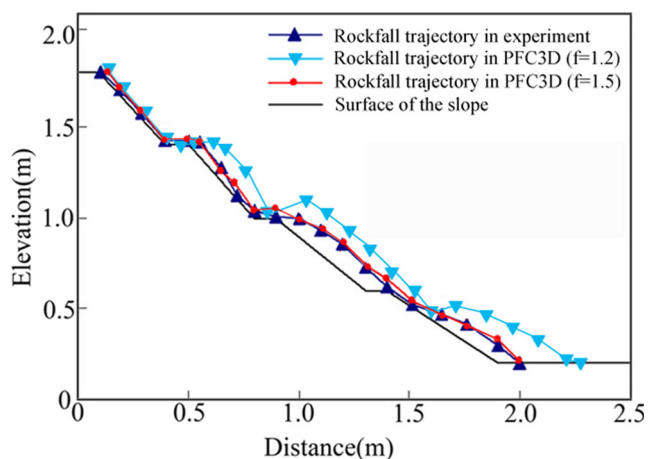


Fig. 8 Comparison of rockfall trajectory between the laboratory experiment and the PFC3D

steps: (1) the association between the configuration of baffles and its energy-dissipating capacity; (2) the association between baffle configuration and the areas affected by avalanche; the specific association between baffle configuration and damage resistance.

Before the case studies, some assumptions were made based on results from previous studies (Choi et al. 2014). First, we assumed that all structures in PFC3D are made up of wall elements, such that building structure failure need not to be taken into consideration. Under this assumption, the study focused on a number of technical problems, such as the configuration of the specific system and its efficiency for energy dissipation.

Influence of baffle configuration

The main factor determining baffle configuration is the density. We considered three baffle densities in our study, namely, high, medium, and low density (shown as S1, S2, and S3, respectively, in Fig. 5).

Figure 12 shows a comparison of the velocity magnitudes of a rock avalanche at the three baffle densities and without baffles, with the distribution of each fragment of rock avalanches, along with different time steps. The velocity contour of avalanches that moved without any interference from baffles lasted the longest, while the velocity contour of

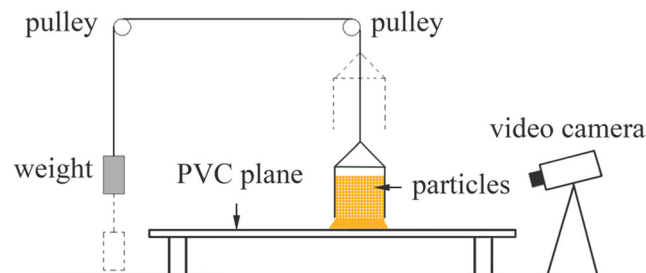


Fig. 9 Scheme of the experimental set-up. *PVC* polyvinyl chloride

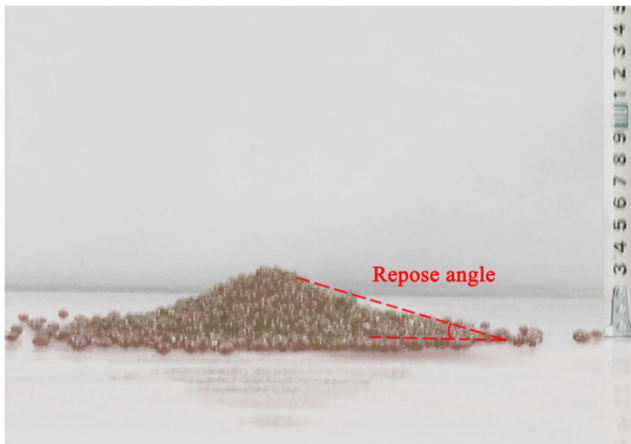


Fig. 10 Final deposition of the granular column with granitic particles

avalanches which moved through baffles sustained short-term changes. It should also be noted that the greater the density, the shorter the velocity changes sustained. Figure 12 also reflects the final deposition of the avalanches in different situations, with the final deposition of avalanches that moved without interference from baffles distributed mainly in the toe of slope, while those moving through a baffle system distributed mainly in region C where the baffles were constructed.

Influence of baffle configuration on the ability to dissipate energy

The energy of rock avalanches in the source area is potential energy, which converts to kinetic energy when triggered by, for example, an earthquake or rainfall. As the changing rule of velocities can reflect the changing rule of kinetic energy, we

conducted a series of numerical experiments that reflect the changes in the velocity of avalanches with different baffle configurations.

In this study, we make reference to the analysis method of granular flow kinetics proposed by Savage and Hutter (1989). This method considers that the common expression form of granular flow kinetics can transform into a non-dimensional expression form. Thus, despite the size effect in the source area, granular flow in different scales can be compared through the non-dimensional expression. The dimensionless forms of travel time and travel velocity can be written as:

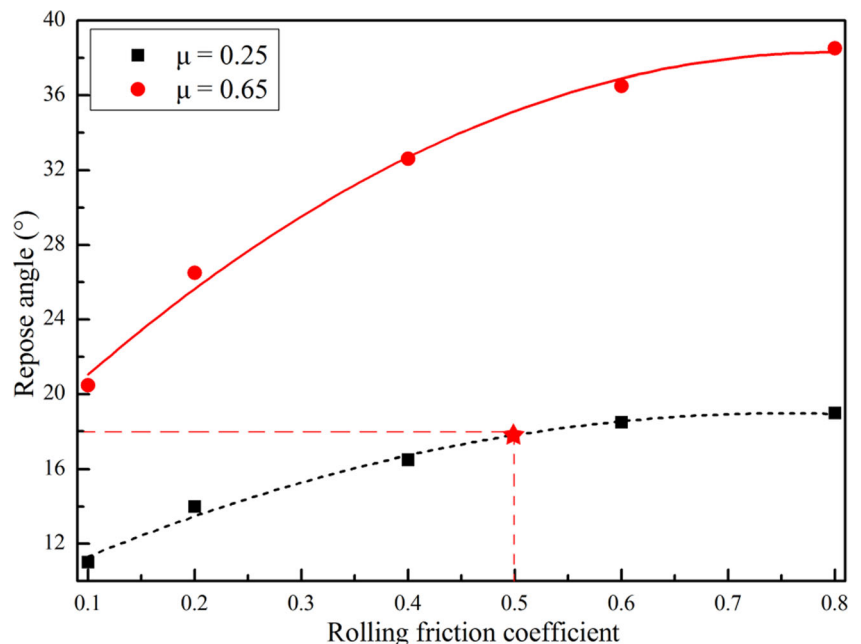
$$t^* = \frac{t}{\sqrt{L_0/g}}$$

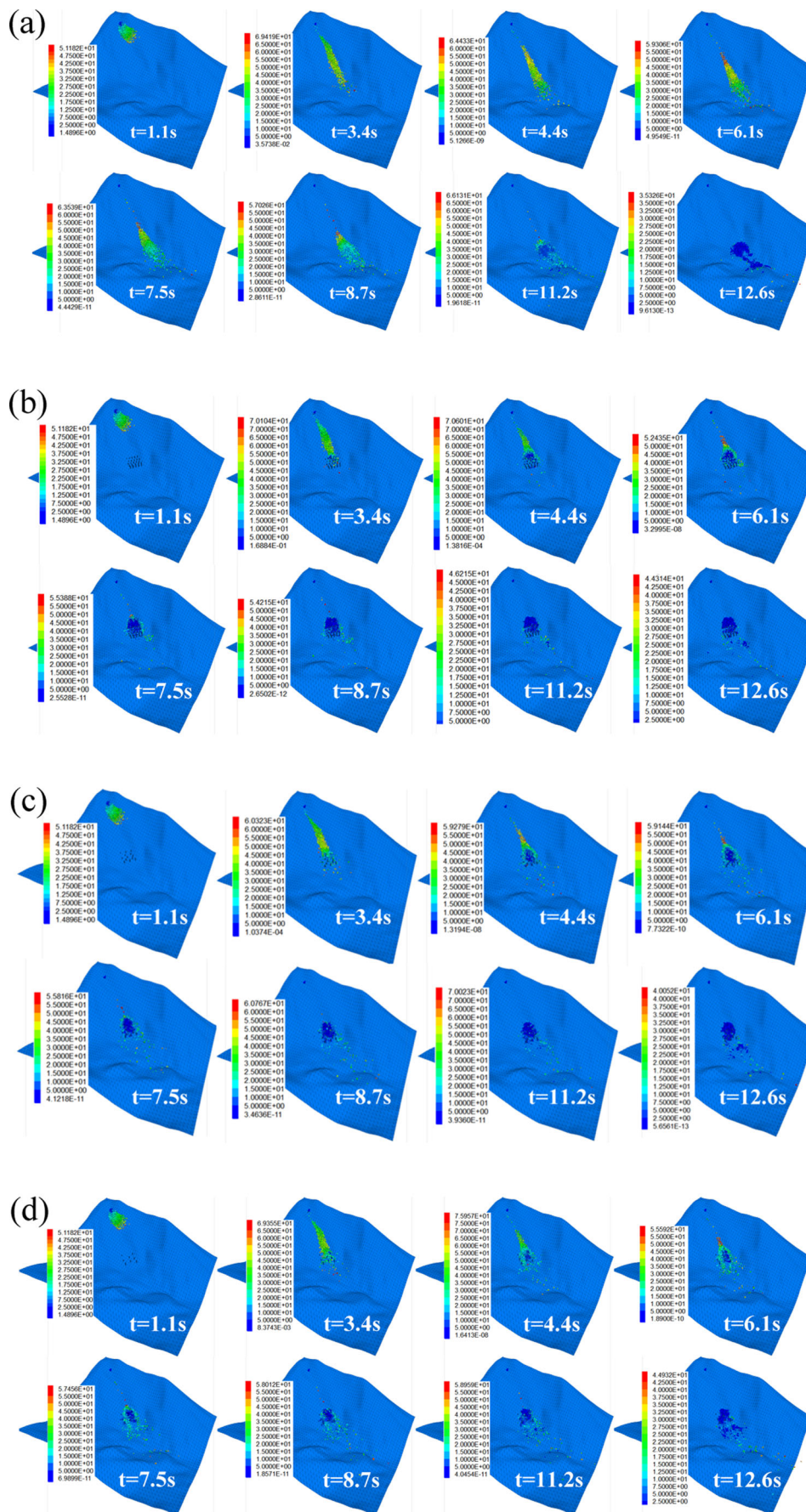
$$U^* = \frac{U}{\sqrt{gL_0}}$$

where t^* is the non-dimensional travel time, t is the normal form of travel time, U^* is the dimensionless form of travel velocity, U is the normal form of travel velocity, g is the gravitational acceleration, and L_0 is the length of granular.

Figure 13 shows the variation in the front velocity and tail velocity of the avalanches with respect to baffle configuration, together with the time steps. Figure 10a–d depicts the change in avalanche velocity in numerical conditions of no baffles and the S1, S2, and S3 configurations, respectively. The process of velocity changes can be divided into two stages: acceleration stage and deceleration stage. A comparison of the deceleration stage for all baffle configurations reveals that the slope change of the curve is the strongest for configuration S1 and the gentlest when no baffles are present. In addition, the slope change is much more obvious at greater baffle density

Fig. 11 Variation of repose angle with changes in the rolling friction coefficient μ_r for different friction coefficients μ





◀ **Fig. 12** Comparison of velocity magnitudes of avalanches. **a** Simulation without the baffles, **b** simulation with the baffles series S1, **c** simulation with the baffles series S2, **d** simulation with the baffles series S3. See Fig. 5 for configurations of S1–S3

because beside the energy loss in the impact with the baffles, avalanche fragments will block the interspace between baffles and change the original motion of the avalanche’s flow. As shown in Fig. 9, two bypasses around the region C are formed due to fragment blocking. In addition, the flow rate of avalanches decreases as the baffle density increases.

Influence of baffle configuration on area affected by avalanches

The relationship between baffle configuration and the area affect by avalanches in this region is shown in Fig. 14. Figure 14a shows the relationship between the area affected

by avalanches and the residential area in the simulation with no baffles (red: area affected by avalanches; white loop: residential). Clearly, in this simulation, one-quarter of the land on the residential area was affected by avalanches.

Figures 14b and 14 c, d, e show the final depositions of avalanches under the conditions of no baffles and baffles at configuration S3, S2, and S1, respectively. It is notable that the deposition amount in region C increases with increasing baffle density. Nevertheless, residential area remains under the threat of rock avalanches in all scenarios.

Influence of baffle configuration on avalanche impact force

In practical engineering, standard approaches employed to design protective obstacle systems are mainly based on the assessment of the impact force caused by avalanche fragments, as well as the lower impact force. The maximum impact force is usually regarded as a crucial index that closely

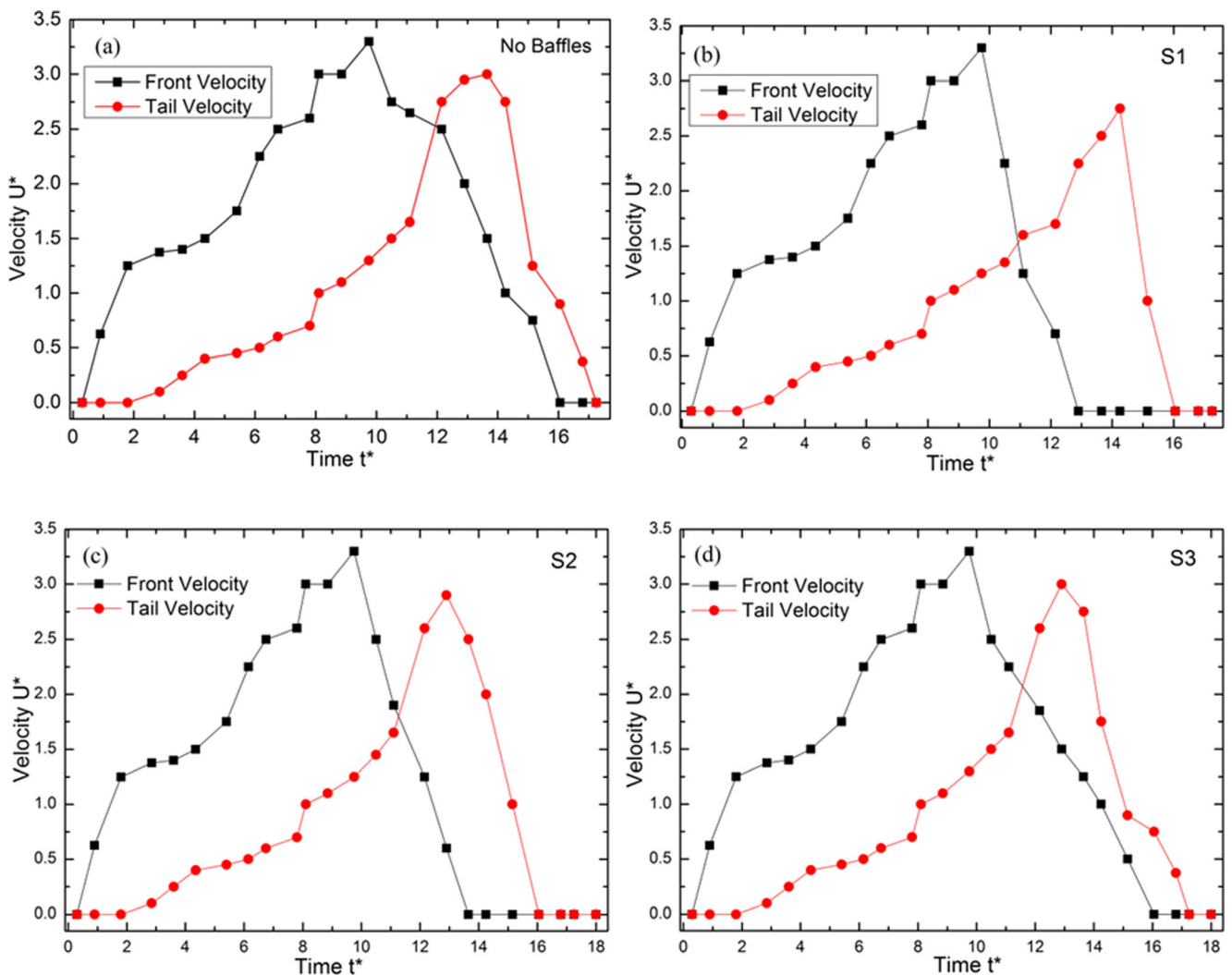
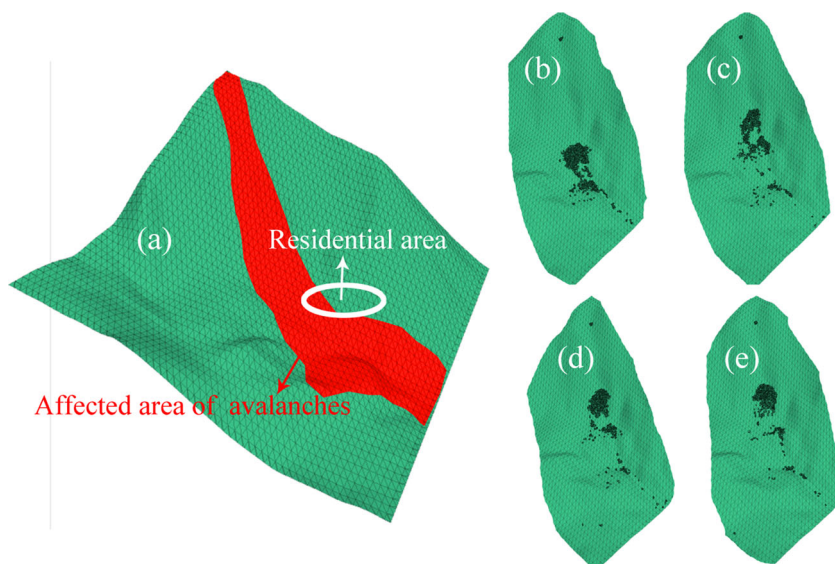


Fig. 13 Relationship between velocities and time step with non-dimensional expression. t^* Non-dimensional travel time, U^* dimensionless form of travel velocity

Fig. 14 Area affected by avalanches and final depositions. **a** Relationship between affected area and residential area, **b** final deposition with no baffles, **c** final deposition with baffles in configuration S1, **d** final deposition with baffles in configuration S2, **e** final deposition with baffles in configuration S3



reflects the defending structures' damage resistance in association with construction costs.

Figure 15 shows the average impact force exerted on each baffle of each row with different configurations. Linear change with change in baffle density is clearly visible, with the average impact force exerted on baffles becoming smaller with increasing baffle density. The maximum impact force exerted on each single baffle at different baffle densities is shown in Fig. 16. In the situation of configuration S1, the maximum impact forces exerted on each single baffle in row (R)1 and R2 are much higher than those exerted on subsequent rows. However, in configurations S3 and S2, the value of the maximum impact forces in R1 and R2 is similar to that in subsequent rows. The explanation for this difference is that increases in baffle density will enhance the extent of blockage by the avalanche; consequently, avalanches up-stream cannot pass

through the former baffles and consequently impinge on the subsequent baffles, thereby limiting their effectiveness in dissipating avalanche energy.

Influence of baffle configuration on avalanche wall

Avalanche walls in the run-out areas of debris flow or snow avalanches are widely employed as protection measures against landslide hazards in different scales. The length and height of the wall are the main factors that influence the capacity of the wall to dissipate energy. As the factor of height is not considered in this study because the overflowed rock mass will impinge the residential area behind the wall, we considered two scenarios related to the factor of wall length: (1) wall W₁ with sufficient length to block all the avalanche fragments; (2) wall W₂ that only blocks part of the avalanche fragments but the residential area is still protected.

Figure 17 illustrates the force evolution with structure change when different wall sizes are applied. It also shows that the peak force in scenario W₁ is much lower than that in scenario W₂. The explanation for this difference is that those parts of the rock avalanche bypass the barrier and thereby take away some of the kinetic energy in the W₂ scenario; thus, the impact force exerted on W₂ will be lower than that exerted on W₁.

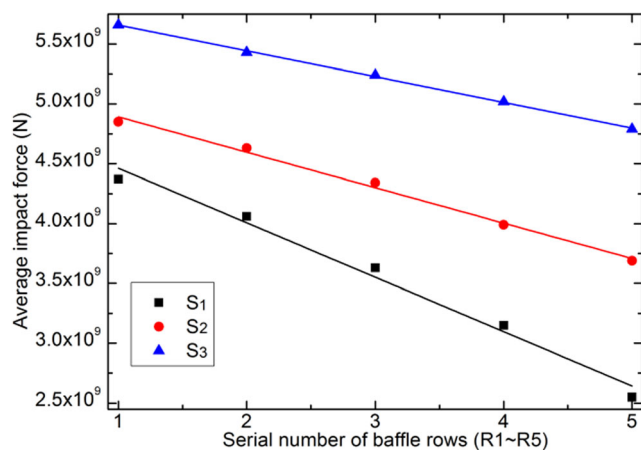


Fig. 15 Average impact force exerted on each baffle row with different baffles density. *R* Row

Influence of baffles–avalanche wall mixed configuration

Protecting baffles and avalanche walls have their own unique advantages in practical engineering. Baffle structure can effectively dissipate the kinetic energy of the hazard, whereas with no spacing between two baffles, a wall structure can effectively block the rock masses and provide enhanced protection to the target areas. Therefore, combining these structures into a

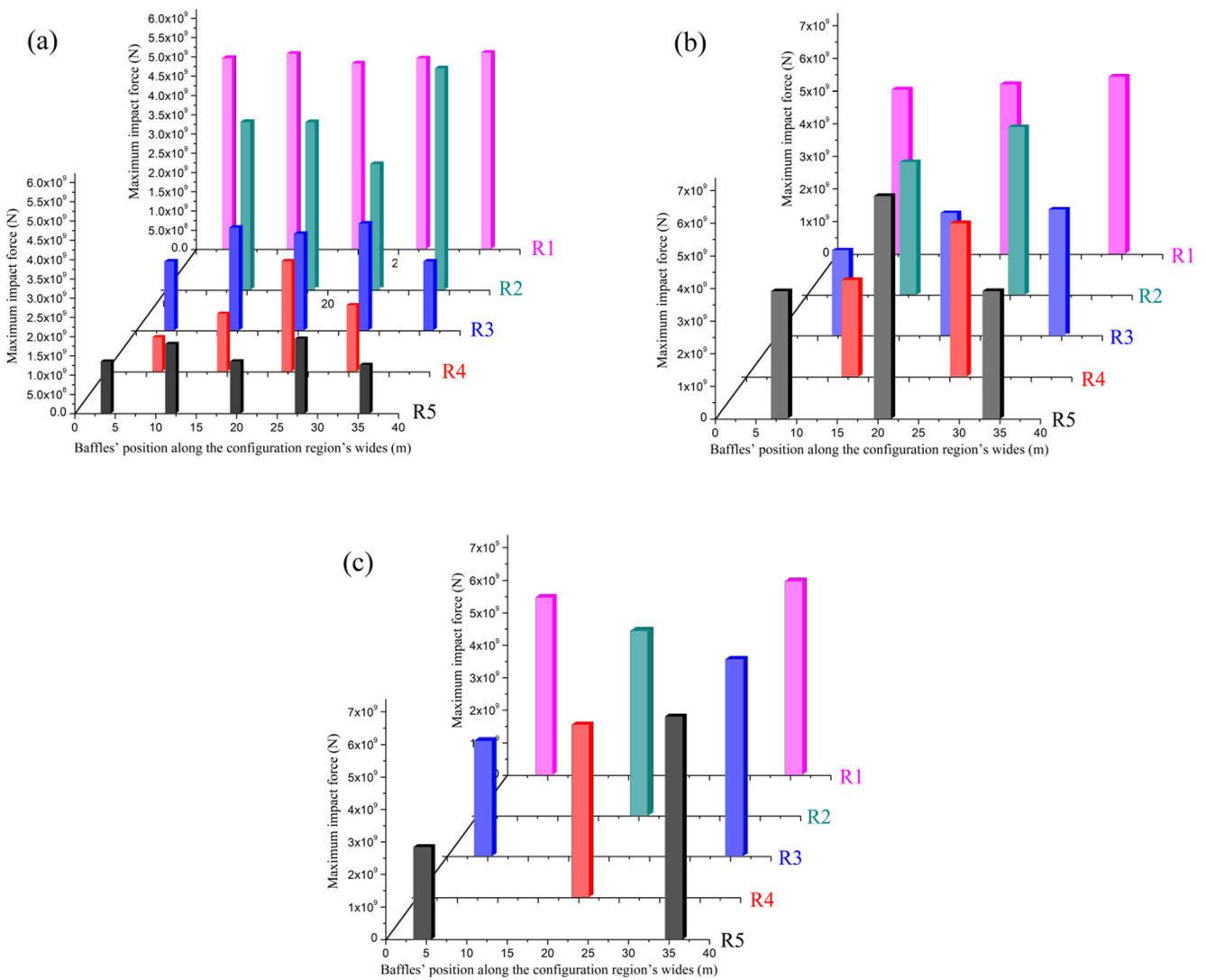


Fig. 16 Maximum impact force exerted on a single baffle. **a** Baffle configuration S1, **b** baffle configuration S2, **c** baffle configuration S3

combined avalanche protection system has advantages in the context of practical engineering that are very significant.

Figure 18 illustrates the maximum impact force evolution exerted on the avalanche wall along with number of baffle rows

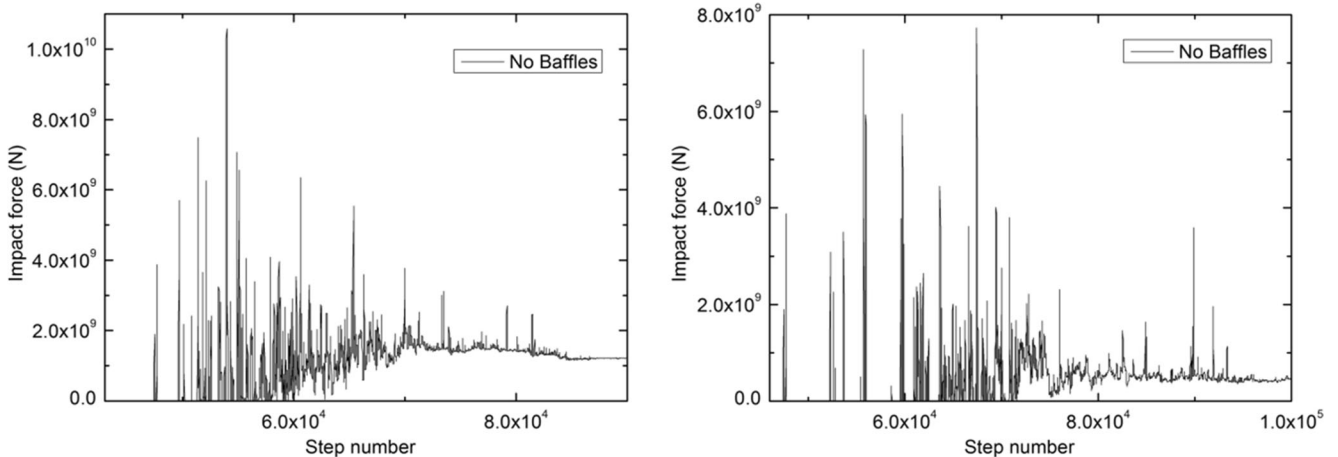


Fig. 17 Impact forces exerted on the avalanche wall at different wall size and step number. Left: Impact forces exerted on wall W_1 , right: impact force exerted on wall W_2 . See text for explanation of W_1 and W_2

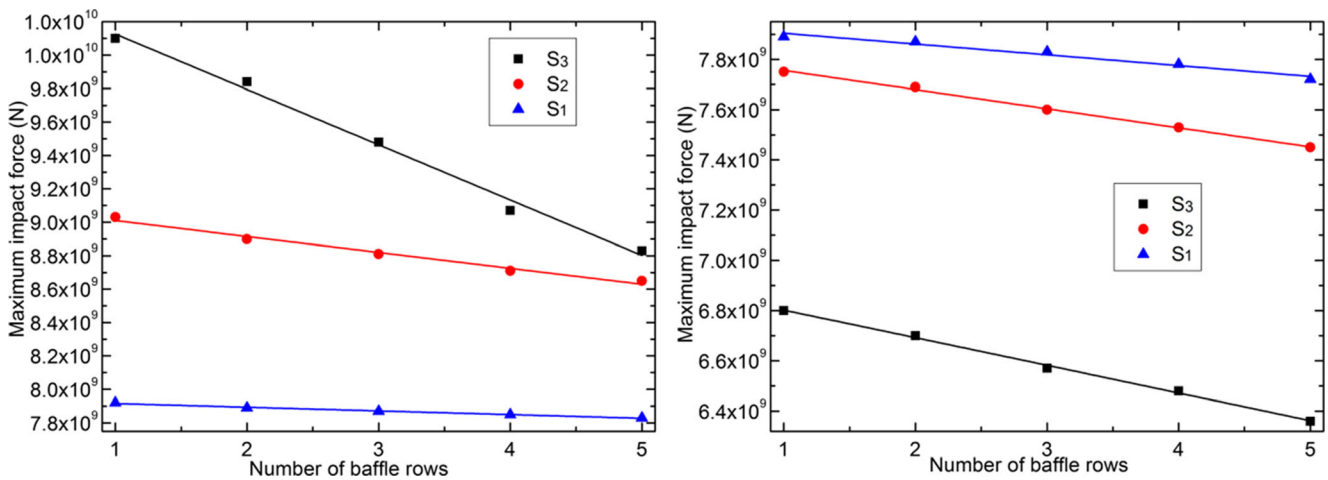


Fig. 18 Maximum impact forces exerted on avalanche walls at different baffle densities and number of baffle rows. Left: With wall W_1 , right: with wall W_2

when different baffle densities are applied. The left figure is the scenario of avalanche wall W_1 and the right figure is the scenario of avalanche wall W_2 . It is evident from both figure parts that the density of the baffles dramatically affects the maximum impact force; nonetheless, the rules in these two figures are totally different. As demonstrated in Fig. 18 (left), at the baffle density of configuration S1, the maximum impact force exerted on the avalanche wall is much lower than that exerted on the wall with baffle configurations S2 and S3. However, as demonstrated by Fig. 18 (right), at the baffle density of S3, the maximum impact force exerted on the avalanche wall is much lower than that at S1 and S2. Furthermore, both Fig. 18 (left) and (right) indicates that the maximum impact force declines with increasing number of baffle rows.

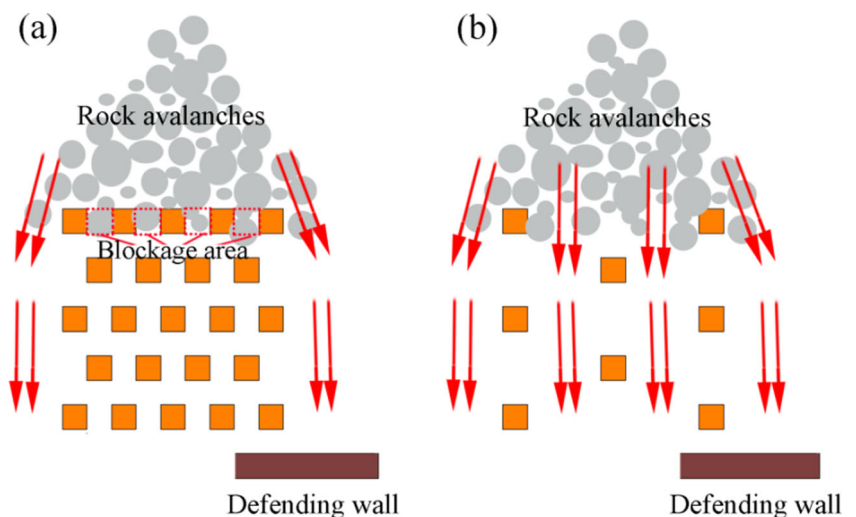
These results verify that baffle density and wall size function together to influence the result of avalanche energy dissipation. The different results are mainly due to the following:

- (1) A reduction in baffle density will decrease the extent of fragment blockage; subsequent avalanches will cross

region C easier at lower baffle density than when baffle density is greater. Hence, the collision probability between fragments and baffles will decrease; meanwhile, the capacity of energy dissipation will decrease. Thus, with all avalanches blocked by the avalanche wall in Fig. 18 (left), an increase in baffle density will reduce the maximum impact force.

- (2) A reduction in the wall size will also decrease the extent of fragment blockage; subsequent avalanches that cross region C with an amount of kinetic energy will bypass the avalanche wall, causing a loss of kinetic energy. Avalanches up-stream will also bypass region C when this region is blocked, as demonstrated in Fig. 19a. As the baffle density decreases, the possibility that avalanches cross region C is enhanced, as shown in Fig. 19b; the capacity of energy dissipation will then decrease. Thus, with part of the avalanches blocked by the avalanche wall in Fig. 18 (right), a decrease in baffle density will reduce the maximum impact force.

Fig. 19 Avalanche movement with different types of baffles—avalanche wall configuration. **a** With baffles in configuration S1, **b** with baffles in configuration S2



Conclusions

A series of in-depth studies on the prevention and mitigation of rock avalanches has been conducted, based on the practical engineering background of the town of Zhangmu, Tibet. This study mainly focuses on an investigation of the configuration of the baffles–avalanche wall mixed system in terms of impedance of rock avalanches. To illustrate this problem specifically, the study was conducted in three steps. First, studies on baffle configuration and its effect on the impedance of rock avalanches were conducted. Secondly, the relationship between the size of the avalanche wall and the maximum impact force of the rock collapse disaster was studied. Lastly, studies on baffles–avalanche wall mixed systems and their energy dissipation capacity were conducted. The impact force exerted on these systems was also studied.

Applying the 3D DEM method, we conducted a series of numerical experiments, which revealed that two main factors are involved in the energy dissipation of the rock avalanche: the density of the pile and the size of the avalanche wall. Increasing the density of the pile will increase its ability to dissipate the energy of the rock collapse so that the ability of the rock collapse to pass through the pile will be weakened. Both of these factors are very crucial when the avalanche wall was added as defending structure, especially in wall series W2. Dense baffles will cause fragment blockage, and subsequent avalanches will bypass this region. However, rock avalanches will pass through the sparse baffles more easily, resulting in higher kinetic energy loss and a lower maximum impact force exerted on avalanche wall W2.

It is important to note that the conclusions drawn here and results presented are applicable only to the situations of specific practical engineering similar those found in the town of Zhangmu, Tibet. Further study is needed to broaden the application scope of these findings.

Acknowledgments The authors gratefully acknowledge financial support from the Project of National Science Foundation of China (Grant No: 41472325, Grant No. 41472293, Grant No. 91430105). This research has also received financial support from the Sichuan Science and Technology Support Program (Grant No. 2016SZ0067).

References

- Ai J, Chen J-F, Rotter JM, Ooi JY (2011) Assessment of rolling resistance models in discrete element simulations. *Powder Technol* 206(3): 269–282
- Aydan Ö (2016) Some considerations on a large landslide at the left Bank of the Aratozawa dam Caused by the 2008 Iwate–Miyagi intraplate earthquake. *Rock Mech Rock Eng* 49(6): 2525–2539
- Azzoni A, De Freitas MH (1995) Prediction of rockfall trajectories with the aid of in situ test. *Rock Mech Rock Eng* 28(2):111–124
- Bi Y, He S, Li X et al (2016a) Effects of segregation in binary granular mixture avalanches down inclined chutes impinging on defending structures. *Environ. Earth Sci* 75(3):263
- Bi Y, He S, Li X et al (2016b) Geo-engineered buffer capacity of two-layered absorbing system under the impact of rock avalanches based on discrete element method. *J Mt Sci* 13(5):917–929
- Bi Y, Du Y, He S, Sun X, Wang D, Li X, Liang H, Wu Y (2018) Numerical analysis of effect of baffle configuration on impact force exerted from rock avalanches. *Landslides* 15(5):1029–1043
- Choi CE, Ng CWW, Law RPH et al (2014) Computational investigation of baffle configuration on impedance of channelized debris flow. *Can Geotech J* 52(2):182–197
- Cosenza E, Cozzolino L, Pianese D, Fabbrocino G, Acanfora M (2006) Concrete structures for mitigation of debris-flow hazard in the Montoro Inferiore Area, Southern Italy. 2nd International Congress, IFSC, Naples, pp 1–12
- Cox SC, Allen SK (2009) Vampire rock avalanches of January 2008 and 2003, southern alps, New Zealand. *Landslides* 6(2):161–166
- Cundall PA, Strack ODL (1979) A discrete numerical model for granular assemblies. *Geotechnique* 29(1):47–65
- Davies TR, McSaveney MJ (1999) Runout of dry granular avalanches. *Can Geotech J* 36(2):313–320
- Davies TR, McSaveney MJ (2002) Dynamic simulation of the motion of fragmenting rock avalanches. *Can Geotech J* 39(4):789–798
- Denlinger RP, Iverson RM (2004) Granular avalanches across irregular three-dimensional terrain: 1. Theory and computation. *J Geophys Res Earth Surf* 109:F1. <https://doi.org/10.1029/2003JF000085>
- Grämiger LM, Moore JR, Vockenhuber C et al (2016) Two early Holocene rock avalanches in the Bernese alps (Rinderhorn, Switzerland). *Geomorphology* 268:207–221
- He SM, Liu W, Wang J (2015) Dynamic simulation of landslide based on thermo-poro-elastic approach. *Comput Geosci* 75:24–32
- Hung O, Evans SG (2004) Entrainment of debris in rock avalanches: an analysis of a long run-out mechanism. *Geol Soc Am Bull* 116(9–10):1240–1252
- Hung O, Leroueil S, Picarelli L (2014) The Varnes classification of landslide types, an update. *Landslides* 11(2):167–194
- Itasca Consulting Group Inc (2016) PFC3D particle flow code in 3 dimensions. User's guide. Itasca Consulting Group Inc, Minneapolis
- Jóhannesson T, Gauer P, Issler P, et al (2009) The design of avalanche protection dams: recent practical and theoretical developments. Office for Official Publications of the European Communities, Luxembourg. <https://doi.org/10.2777/12871>
- Li B, Xing A, Xu C (2017) Simulation of a long-runout rock avalanche triggered by the Lushan earthquake in the Tangjia Valley, Tianquan, Sichuan, China. *Eng Geol* 218:107–116
- Li X, He S, Luo Y et al (2010) Discrete element modeling of debris avalanche impact on retaining walls. *J Mt Sci* 7(3):276–281
- Liu W, He S (2018) A two-layer model for the intrusion of two-phase debris flow into a river. *Q J Eng Geol Hydrogeol* 51(1):113–123
- Mollon G, Richefeu V, Villard P et al (2015) Discrete modelling of rock avalanches: sensitivity to block and slope geometries. *Granul Matter* 17(5):645–666
- Ng CWW, Choi CE, Kwan JSH et al (2014) Effects of baffle transverse blockage on landslide debris impedance. *Proc Earth Planet Sci* 9:3–13
- Ng CWW, Choi CE, Song D et al (2015) Physical modeling of baffles influence on landslide debris mobility. *Landslides* 12(1):1–18
- Qi S, Xu Q, Zhang B et al (2011) Source characteristics of long runout rock avalanches triggered by the 2008 Wenchuan earthquake, China. *J Asian Earth Sci* 40(4):896–906
- Salciarini D, Tamagnini C, Conversini P (2009) Numerical approaches for rockfall analysis: a comparison. Proceedings of the 18th International Congress on Modelling and Simulation, Cairns, Australia, p 2706–2712
- Savage SB, Hutter K (1989) The motion of a finite mass of granular material down a rough incline. *J Fluid Mech* 199:177–215

- Strom AL (2004) Rock avalanches of the Ardon River valley at the southern foot of the rocky range, northern Caucasus, north Osetia. *Landslides* 1(3):237–241
- Tokashiki N, Aydan Ö (2011) Kita-Uebaru natural rock slope failure and its back analysis. *Environ Earth Sci* 62(1):25–31
- Ulusay R, Aydan Ö, Kılıç R (2007) Geotechnical assessment of the 2005 Kuzulu landslide (Turkey). *Eng Geol* 89(1–2):112–128
- Wensrich CM, Katterfeld A (2012) Rolling friction as a technique for modelling particle shape in DEM. *Powder Technol* 217:409–417
- Xing A, Yuan X, Xu Q, et al (2017) Characteristics and numerical runout modelling of a catastrophic rock avalanche triggered by the Wenchuan earthquake in the Wenjia valley, Mianzhu, Sichuan, China. *Landslides* 14(1):83–98